Geodesy and Geodynamics 14 (2023) 212–222

Contents lists available at ScienceDirect

Geodesy and Geodynamics

journal homepage: http://www.keaipublishing.com/geog

Coastal bathymetry inversion using SAR-based altimetric gravity data: A case study over the South Sandwich Island

Yihao Wu [a], Junjie Wang [a, *], Xiufeng He [a], Yunlong Wu [b], Dongzhen Jia [a], Yueqian Shen [a]

[a] School of Earth Sciences and Engineering, Hohai University, Nanjing 211100, China
[b] Key Laboratory of Geological Survey and Evaluation of Ministry of Education, China University of Geosciences, Wuhan 430079, China

ARTICLE INFO

Article history:
Received 24 June 2022
Accepted 8 October 2022
Available online 6 November 2022

Keywords:
Coastal bathymetry inversion
Synthetic aperture radar altimeter
Sentinel-3A/3B
CryoSat-2
Altimetric gravity data
Scale factor

ABSTRACT

The global bathymetry models are usually of low accuracy over the coastline of polar areas due to the harsh climatic environment and the complex topography. Satellite altimetric gravity data can be a supplement and plays a key role in bathymetry modeling over these regions. The Synthetic Aperture Radar (SAR) altimeters in the missions like CryoSat-2 and Sentinel-3A/3B can relieve waveform contamination that existed in conventional altimeters and provide data with improved accuracy and spatial resolution. In this study, we investigate the potential application of SAR altimetric gravity data in enhancing coastal bathymetry, where the effects on local bathymetry modeling introduced from SAR altimetry data are quantified and evaluated. Furthermore, we study the effects on bathymetry modeling by using different scale factor calculation approaches, where a partition-wise scheme is implemented. The numerical experiment over the South Sandwich Islands near Antarctica suggests that using SAR-based altimetric gravity data improves local coastal bathymetry modeling, compared with the model calculated without SAR altimetry data by a magnitude of 3.55 m within 10 km of offshore areas. Moreover, by using the partition-wise scheme for scale factor calculation, the quality of the coastal bathymetry model is improved by 7.34 m compared with the result derived from the traditional method. These results indicate the superiority of using SAR altimetry data in coastal bathymetry inversion.

1. Introduction

Coastal seabed topography over polar areas is critical for tracking the dynamic changes in polar climate as well as evaluating the melting rate of polar glaciers and assessing the impact on polar biological systems [1–4]. In addition, the fishing industry, oil exploitation, and coastal traffic are notable examples in which seabed topography substantially impacts human production and life [5–7]. The development of the bathymetry model over polar areas is mainly based on shipborne soundings data and bathymetry data derived from gravity data [8,9]. The shipborne sounding technique is an efficient way to measure seafloor topography, with an accuracy better than 0.25 m in shallow water and less than 0.5 m in deep water [10].

However, the shipborne measurements derived from single-beam and multi-beam soundings are difficult to cover most polar areas due to the harsh environment, massive glacier coverage, and complex seafloor topography. As a result, the sea depths are usually filled with bathymetry information computed from altimetric gravity data [11]. With the development of satellite altimetry technology, the accuracy of the altimetric gravity field model has also been improved [12,13]. However, the altimetric gravity data computed from the conventional altimeter data is usually of low accuracy due to waveform contamination over coastal regions, and data gaps exist near offshore areas in polar regions [14,15]. As a result, acquiring high-precision altimetric gravity data is the key to improving the accuracy of coastal bathymetry modeling.

The use of synthetic aperture radar (SAR) altimeter data alleviates the problem of low quality of conventional satellite altimetry over offshore regions. The SAR altimeter utilizes time-delayed

* Corresponding author.
E-mail address: junjie2020@hhu.edu.cn (J. Wang).

Peer review under responsibility of Institute of Seismology, China Earthquake Administration.

Production and Hosting by Elsevier on behalf of KeAi

https://doi.org/10.1016/j.geog.2022.10.001

Doppler technology to capture more radiant energy and receive high pulse repletion frequency signal based on full decamp technology [16]. The raw echo signal received in the SAR altimeter is transformed into a two-dimensional data matrix to form striped area information using the power spectrum, beam steering, or Doppler position map [17]. This mode in SAR altimeter can considerably improve the precision of height measurement in comparison with traditional real aperture altimeter [18–20].

The study from Xu et al. showed that the accuracy of sea surface height measurement derived from SAR altimeter was about one time higher than that retrieved from traditional altimeter [21]. Wu et al. highlighted the advantage of using SAR altimeter data in local marine gravity field recovery over coastal areas [22]. Labroue et al. suggested that the SAR altimeter on CryoSat-2 mission improved the accuracy in waves and sea level anomaly applications over sea surface, with a standard deviation of approximately 6.5 cm [23]. These results inspire us to study the contribution of seabed terrain inversion based on SAR altimeter data. Therefore, this study focused on applying SAR altimetry data (such as Sentinel-3A/3B [24,25]) in coastal bathymetry modeling over polar regions.

The bathymetry can be modeled based on the frequency domain approach (S&S method), which does not rely on prior geophysical information and ensures the accuracy of the computed model [26–28]. The determination of the scale factor between bathymetry and gravity anomaly is the key issue. The typical method for scale factor determination is based on the RANdom SAmple Consensus (RANSAC) algorithm; however, it may result in an inability to accurately reflect seafloor topography changes in the regions with significant topographic undulation [29]. Ashalatha studied the specific fractal analysis method to calculate the scale factor, which involved calculating the horizontal and vertical scale factors on the profile [30]. Sun et al. employed partition scale factor calculation to model bathymetry over the South China Sea, segmenting the entire study area with a fixed scale factor calculation window (resolution of 1°) [31]. Considering the undulating topography over the South Sandwich Islands areas, we implement a polynomial fitting method for scale factor determination in this study, where the partition-wise scheme is used in this method.

The sections of this study are mentioned below: the method for bathymetry determined from gravity data is briefly introduced in section 2. The definition of truncation wavelength and the approach to estimating scaling factors are introduced. The study region and data sets utilized for local bathymetry modeling and validation are described in section 3. The numerical experiments are presented in section 4, and the effects introduced from the SAR altimetry data on coastal bathymetry inversion are quantified and evaluated. The summary and conclusion are presented in section 5.

2. Method

Based on Parker's formula [32], we model the coastal bathymetry with altimetric gravity models, and the scale factor is computed from the linear relationship between bathymetry and gravity anomaly in the frequency domain. The details of this method can be seen in Smith's study [26]. The flow chart in Fig. 1 displays the bathymetry inversion from altimetric gravity data and the reference bathymetry model.

2.1. The choice of band-pass filter in bathymetry inversion

The initial stage in bathymetry modeling from gravity data is to process the bathymetry and gravity data in the frequency domain. The research from Smith and Sandwell suggested that bathymetry and gravity data were substantially correlated in the frequency band with the wavelength from 15 to 160 km, which could be linked by a scale factor [26]. The acquisition of the band-pass filtered signal can be determined by the truncation wavelength, including the maximum and minimum truncation wavelengths, which are the key parameters in bathymetry inversion. The truncation wavelengths affect the frequency properties of the truncated gravity and bathymetry signals. Moreover, these parameters vary with respect to the study regions, different input gravity data sets, and various reference bathymetry models. Thus, we determine the truncation wavelength parameters based on a trial-and-error method in this study.

Combining the cosine filter and Wiener low-pass filter is used to filter the bathymetry and gravity data. Adili et al. found that the bathymetry modeled with a combined cosine filter produced better results than that modeled with a Gaussian band-pass filter [33]. The cosine filter's general statement is

$$W_{\cos}(k) = 0.5 \times \left[1 + \cos\left(\pi \cdot \frac{k - k_m}{k_s - k_m}\right)\right] \tag{1}$$

where k_m is the wave number of the minimum wavelength in the truncation wavelength range, while k_s is the wave number of the maximum wavelength.

Wiener filter is the low-pass filtering part in the combined cosine filter. The specific expression of the Wiener low-pass filter is

$$W_{\text{wiener}}(k) = \left[1 + Ak^4 \exp(4\pi kd)\right]^{-1} \tag{2}$$

where d is the depth, and A is a parameter in the Wiener filter chosen by the spectral coherence (between gravity anomaly and bathymetry) analysis.

The combined cosine filter based on Eqs. (1) and (2) can be given by

$$W_m(k) = W_{\cos}(k) \cdot W_{\text{wiener}}(k) \cdot \exp(2\pi kd) \tag{3}$$

where d is the depth, and k is the wave number of the gravity anomaly and bathymetry in the frequency domain.

The influence of the maximum and minimum truncation wavelengths on the bathymetry inversion will be investigated in this study, which employs in a combination cosine filter to filter gravity anomaly and bathymetry data in the frequency domain.

2.2. Scale factor calculation

After calculating the filtered gravity anomaly and bathymetry, the scale factor computation is required to determine the ratio relationship between the bathymetry and gravity anomaly. To do this, the RANdom SAmple Consensus (RANSAC) algorithm is usually used. In this method, a representative zone is usually chosen based on the seafloor topographic relief over the study area, and the scale factor derived from the RANSAC algorithm in this region is utilized as the final scale factor for bathymetry inversion over the entire study area. The scale factor mentioned can be computed by using the ratio of the Median Absolute Deviation (MAD) of the band-pass-filtered gravity anomaly and bathymetry data, which can be written as

$$S(x) = \frac{h_{\text{mad}}}{g_{\text{mad}}} \tag{4}$$

where h_{mad} and g_{mad} are the MAD of the band-pass-filtered bathymetry data and gravity anomaly, respectively.

In this paper, we implement a partition scheme for scale factor calculation, compared with the RANSAC method for the bathymetric inversion. The specific method to calculate the scale factor is as

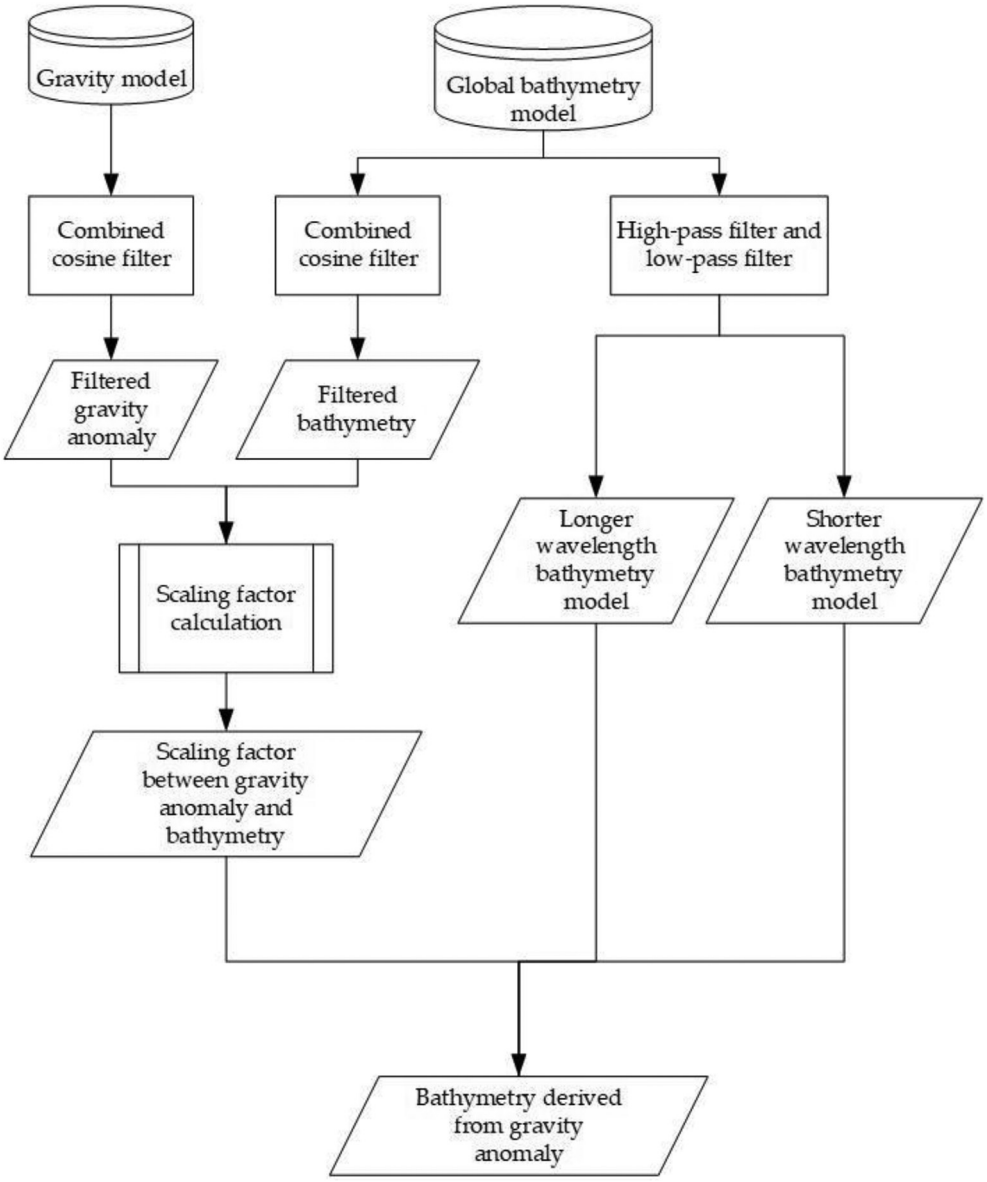

Fig. 1. Flow chart of the bathymetry modeling from gravity anomaly.

follows: 1. The whole research area is divided into equal-spacing grids according to a fixed resolution, which is determined by the seabed topography in the study area; 2. Calculate the scale factor between bathymetry and gravity within each grid region; 3. Calculate the inversion bathymetry in each grid region and merge the inversion bathymetry in the complete study area. The polynomial fitting approach is introduced for scale factor calculation in each grid region. The algorithm for fitting polynomial curves is as follows

$$H_{\mathrm{bp}} = s_0 G_{\mathrm{bp}}^{n} + s_1 G_{\mathrm{bp}}^{n-1} + s_2 G_{\mathrm{bp}}^{n-2} + \cdots + s_n \tag{5}$$

where H_{bp} and G_{bp} are the band-pass filtered bathymetry data and gravity anomaly in each partition regions; $s_0, s_1, s_2, \cdots s_n$ are the fitting value used to calculate the scale factor.

The predicted bathymetry can be expressed as the sum of the longer wavelength of the reference bathymetry model $B_{\mathrm{long}}(x)$, the shorter wavelength of the reference bathymetry model $B_{\mathrm{short}}(x)$, and the medium band of bathymetry signal processed by scale factor $s(x)$, which can be written as the product of scale factor as shown in Eq. (5) and band-pass filtered gravity anomaly $G_{\mathrm{bp}}(x)$. The bathymetry that has been derived can be modeled as

$$H_P(x) = B_{\mathrm{long}}(x) + s(x) \cdot G_{\mathrm{bp}}(x) + B_{\mathrm{short}}(x) \tag{6}$$

where x is the coordinates of the grid nodes in the polar stereoscopic coordinate system; $H_P(x)$ is the value of the derived bathymetry. Fig. 2 shows a flow chart of two different methods to calculate the scale factor between bathymetry and gravity data: on the left, the scale factor calculated using the RANSAC method denoted as Solution A; on the right, the scale factor calculated based on the partition method and polynomial fitting approach, named as Solution B.

3. Data and study area

The study area was centered on two islands in the Southern Ocean (South Georgia and the South Sandwich Islands) near Antarctica, east of South America's southern point and north of

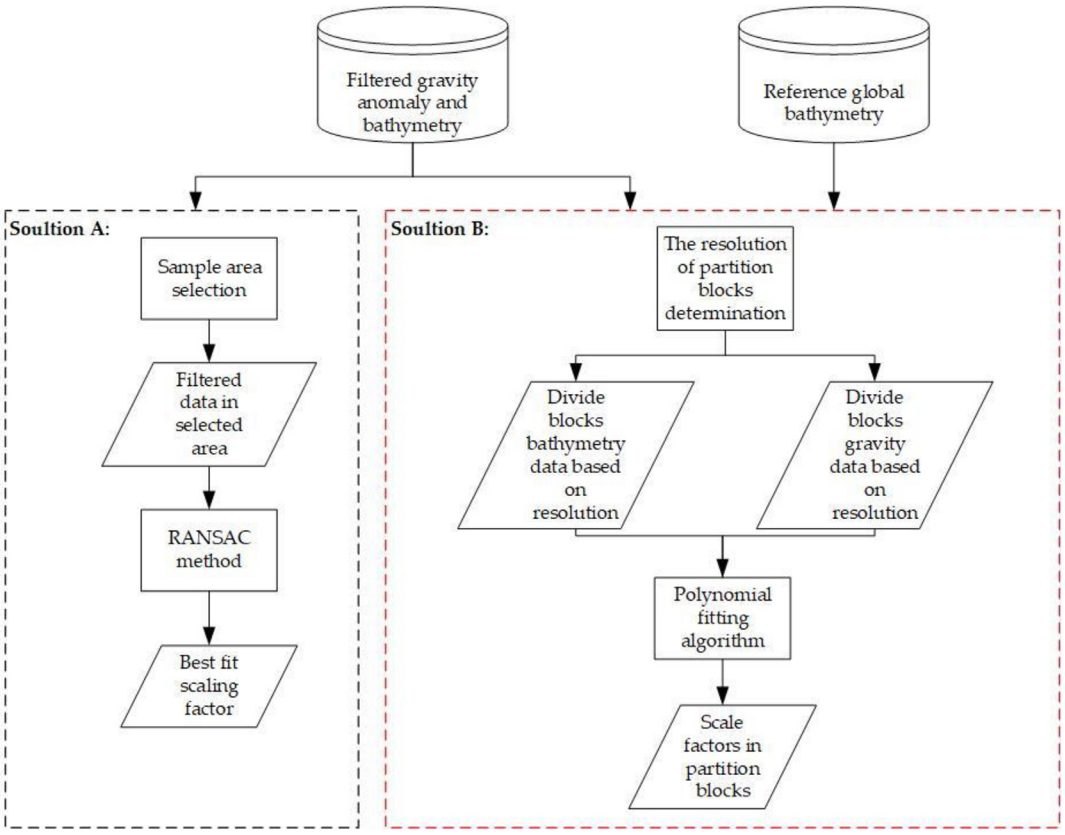

Fig. 2. Flow chart of two schemes to calculate scaling factor.

Antarctica (52–57°S, 30–40°W) (Fig. 3 (a)). On the one hand, because the islands are near the pole and uninhabited, there is a scarcity of shipborne soundings data in the vicinity. On the other hand, the islands are surrounded by glaciers and a huge number of jagged black and clarke rocks, making the landscape in this area extremely complicated. The height difference in this area varies substantially with the addition of the eastern South Sandwich Trench and ocean rise (such as Northwest Georgia Rise and Northeast Georgia Rise), with a maximum height of 1149 m and a maximum depth of 8128 m (Fig. 3 (b)). Because of the high seafloor terrain relief and harsh environment near the polar regions, high-precision altimetric gravity data measurements are unachievable in this area, making the reconstructed bathymetry model insufficiently accurate. Furthermore, the islands occupy the majority of the research region, and the wide coastal area complicates bathymetry modeling with altimetric gravity data. However, it also provides a great research environment for us to investigate how to improve the coastal bathymetry model with SAR altimetry data.

3.1. Choice of reference bathymetry model

The global bathymetry model General Bathymetry Chart of the Oceans 2020 (GEBCO 2020) is used as the reference model in the bathymetry inversion. GEBCO 2020 is a worldwide ocean and land terrain model developed by the International Hydrographic Organization (IHO) and the Intergovernmental Oceanographic

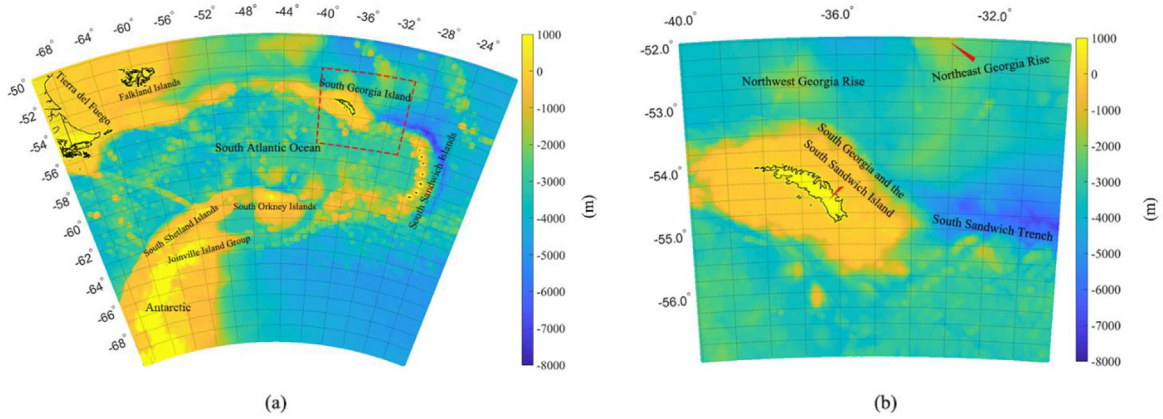

Fig. 3. (a) Location of the study area (region enclosed in the red rectangle) over the South Atlantic Ocean; and (b) distribution of the main seabed topography in the study area.

Commission of UNESCO (IOC). The previous version of the GEBCO model, i.e., GEBCO_2014 is primarily modeled from ship-track soundings data, interpolation data from satellite-derived gravity data, and digital atlas from GEBCO_2008, with a spatial resolution of 30″. The major improvement of GEBCO_2019 over GEBCO_2014 is that the GEBCO_2019 computed with more data from SRTM30+ and with an improved resolution of 15″, while the improvement of GEBCO_2020 over GEBCO_2019 is that the former was modeled utilizing the new version of SRTM15+ data and more soundings data [34].

3.2. Altimetric gravity models

The series of altimetric gravity models established at Technical University of Denmark (DTU) space, namely DTU13GRA, DTU15GRA, DTU17GRA, and DTU21GRA, are used for local bathymetry modeling. These four models all have a spatial resolution of 1 arc-minute. The DTU13GRA model additionally contained three years of CryoSat-2 data (2010–2013) and one year of Jason-1 data (2012–2013) compared with DTU10GRA. The advantage of DTU15GRA over DTU13GRA is that the DTU15GRA is modeled with extra information from Geosat, ERS-1, Cryosat-2, and Jason-1. The main improvement of DTU17GRA over DTU15GRA is that one year of SARAL/AltiKa data (2016–2017) was introduced in DTU17GRA modeling, and more time series of Cryosat-2 data was included [35]. It is noticeable that CryoSat-2 operates in a low-resolution mode over the study area; thus, no SAR altimetry data has been used in the computation of DTU17GRA. Moreover, the improvement of DTU21GRA over DTU17GRA is that the former was modeled utilizing five years of Sentinel-3A and three years of Sentinel-3B data, as well as more Cryosat-2 data disposed by SAMOSA+. Meanwhile, the accuracy of DTU21GRA has significantly improved over the offshore areas in comparison with DTU17GRA due to the introduction of SAR altimeter data [36]. The enhancements to DTU21GRA in short wavelength range, as well as the incorporation of SAR altimetry data like Sentinel-3A/3B, allow us to investigate the impact of SAR altimetry data on coastal bathymetry modeling. As a result, only DTU21GRA is a SAR-based altimetric gravity model among these models.

3.3. Shipborne soundings data

The shipborne soundings data extracted from National Centers for Environmental Information (NCEI, http://www.ncei.noaa.gov/maps/bathymetry/) is used to evaluate the coastal bathymetry modeled with different altimetric gravity models. This shipborne soundings data (survey ID: 19970012) was surveyed by UK Hydrographic Office, and it covers a total of 6370 observation points, with a maximum depth of 3344 m and a minimum depth of 45.90 m after removing aberrant sea depth values in the study region. The coastal bathymetry inversion (within 10 km offshore) will be estimated in the following trials based on the distance between each shipborne measurement location and South Georgia and the South Sandwich Islands.

4. Results and discussions

4.1. The choice of the truncation wavelength

Four generations of DTU altimetric gravity models (DTU13GRA, DTU15GRA, DTU17GRA, and DTU21GRA) were employed as input gravity data in this work. Because a new gravity field model and a reference bathymetric model are used in this study, we are unable to use the parameters of the conventional calculation of the truncated wavelength to improve the accuracy of the bathymetric inversion. We take the "trial-and-error" technique, combining multiple maximum and minimum wavelengths to create a band-pass filter with variable truncation wavelength bands. The results of several band-pass filter truncation wavelengths are compared in this way to determine the best acceptable truncation wavelength. The latest global altimetry gravity field model DTU21GRA is used as the input altimetric gravity model, with a spatial resolution of 1'. It is worth noting that the scale factor in this experiment is calculated using the partition-based method. The partition-based scale factor calculation method is more suitable for this region than the traditional scale factor calculation method because there is a wide range of island topography and a region with a large fluctuation of height difference in the study area; and the specific experimental proof will be given in section 4.2.

The minimum truncation wavelength range was increased from 2 km to 16 km with a 2 km interval, while the maximum truncation wavelength range was altered from 130 km to 200 km with a 10 km increment by the trial-and-error method. The standard deviation (STD) of the mismatches between the bathymetry produced from different truncation wavelength ranges of gravity models and shipborne soundings data can be used to estimate the best-suited truncation frequency in this way. We only use shipborne soundings data in the along track 10 km from the coast to assess the results of the introduction of SAR-based altimetry gravity data in coastal bathymetry retrieval to study the influence of SAR altimetry data in coastal bathymetry retrieval. Fig. 4 depicts the accuracy of multiple models derived with varying truncation wavelengths, with a minimum STD of 23.91 m obtained when the maximum wavelength is 160 km, and the minimum wavelength is 10 km.

The associated statistics are shown in Table 1. We find that changing the maximum truncation wavelength has little effect on the accuracy of coastal bathymetry inversion, especially when the maximum wavelength is greater than 180 km. For example, when the minimum truncation wavelength is fixed at 8 km and the maximum wavelength increases from 180 km to 200 km, the accuracy of the misfits between derived bathymetry and shipborne soundings is pretty much the same. Other results with STD value a few centimeters larger than 23.91 m have slightly worse precision, indicating that the solution is highly stable with respect to modest variations in truncation wavelength parameterization. In contrast to the long wavelength signal, the statistical results show that the medium and short wavelength gravity field model signal is more susceptible to the coastal bathymetry inversion. Because the results indicate that a truncation wavelength range of 10 km–160 km in a band-pass filter is more appropriate for modeling coastal bathymetry, the range of truncation wavelength is chosen from 10 km to 160 km in the following study.

4.2. Scale factor calculation

We further look into the possibility of using appropriate cutoff wavelengths in band-pass filtering to improve the accuracy of bathymetry computations. The method of scale factor computation is a significant aspect that affects the accuracy of coastal bathymetry modeling when we calculate the scale factors between bathymetry and gravity anomaly. In Fig. 2, the RANSAC scaling factor calculation method and the partition scale factor calculation method are shown as Solutions A and B, respectively.

We chose a sample region that spans 53°S to 53.5°S latitude and 35°W to 36°W longitude, comprising the coastline morphology of South Georgia and the South Sandwich Islands, as well as parts of the South Sandwich Trench, for the RANSAC scale factor calculation method. Fig. 5 shows the scaling factors between bathymetry and gravity over the sample region, as calculated from Solution A. The

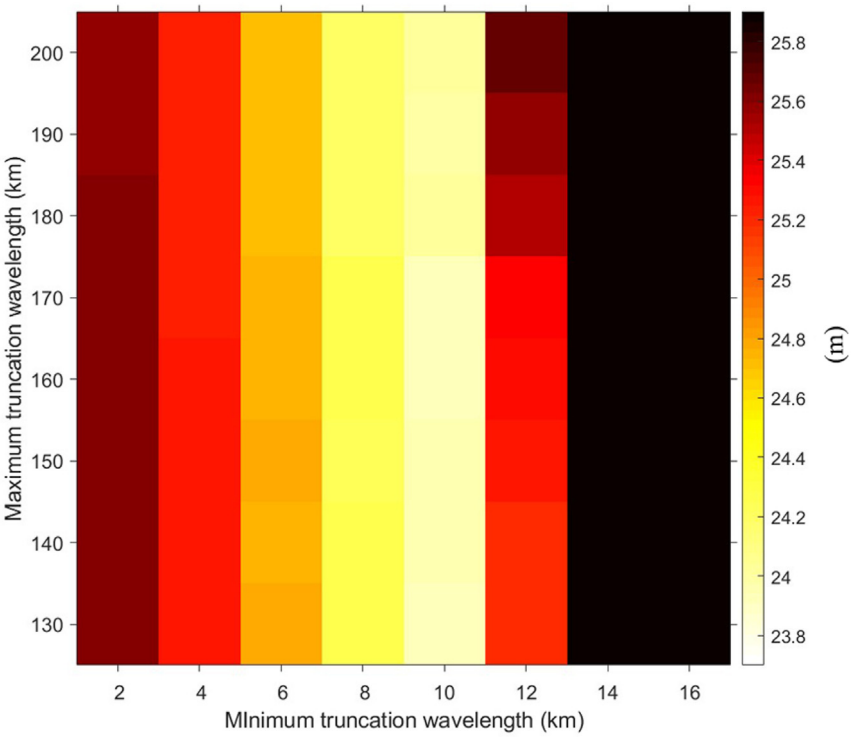

Fig. 4. Accuracy of bathymetry computed from different truncation wavelength range.

distribution of the scale factors between the bathymetry and the gravity anomaly shows an approximately linear relationship. In this method, we determine the fittest scale factor in this sample region by looking for the most "inliers" data and ignoring the "outliers" data. The dispersed blue points show the band-pass-filtered gravity and bathymetry. The scaling factor is calculated using band-pass-filtered gravity and bathymetry in this location, which is represented in Fig. 5 by the slope of the red line that fits the scattered points with a specific value of 8.24 m/mGal.

Because that we only select one sample region to calculate the scale factor based on the RANSAC scale factor calculation approach. As a result, the results of this method may be unable to distinguish between the undulating area of the seabed topography and the special seabed topography (such as trench, sea valley, and ridge). In light of the flaw in Solution A, we consider splitting the research area into grids based on the seafloor topography to calculate the scale factor. The study area is divided into equally-spaced grids according to a fixed resolution, and the scale factors are calculated in each grid area based on the polynomial fitting algorithm. This method, based on partition wise, is named Solution B. At the same time, we evaluate these two methods for scaling factors by calculating the mismatches between bathymetry derived from two solutions and shipborne soundings data.

The associated statistics are shown in Table 2. The results demonstrate that the standard deviation (STD) of the misfits calculated by Solution B is smaller than that estimated by Solution A, which achieves a 7.34 m improvement in bathymetry modeling over the 10 km distances to the coast area. It is worth noting that seabed topography within a 10 km offshore area modeled from Solution B can be distinguished compared with that calculated from Solution A. However, the results calculated from Solution B have a large systematic deviation. The main reason is that GEBCO_2020 contains a deviation in this region. At the same time, the partitioned calculation scale factor method affects the overall error distribution, thus enhancing the bias. Since the results suggest that the partition scale factor calculation method is more appropriate to model the coastal bathymetry compared with the traditional RANSAC method. In the following study, the scaling factor calculation method is chosen partition scale factor calculation method.

The numerical findings show that in areas with considerable seabed topography changes, inversion coastal bathymetry

Table 1
The accuracy of bathymetry derived from various maximum and minimum wavelengths (Units: m).

Minimum truncation wavelength (km)	Maximum truncation wavelength (km)							
	130	140	150	160	170	180	190	200
2	25.62	25.61	25.61	25.61	25.60	25.60	25.59	25.59
4	25.28	25.27	25.27	25.25	25.24	25.23	25.23	25.23
6	24.79	24.76	24.77	24.74	24.75	24.73	24.72	24.73
8	24.28	24.27	24.24	24.26	24.25	24.21	24.21	24.21
10	23.94	23.96	23.95	23.91	23.94	24.02	24.00	24.02
12	25.21	25.21	25.27	25.29	25.34	25.50	25.59	25.67
14	27.05	26.73	26.90	26.98	27.32	27.29	27.23	27.25
16	38.20	38.48	38.19	38.86	38.91	38.20	38.16	38.62

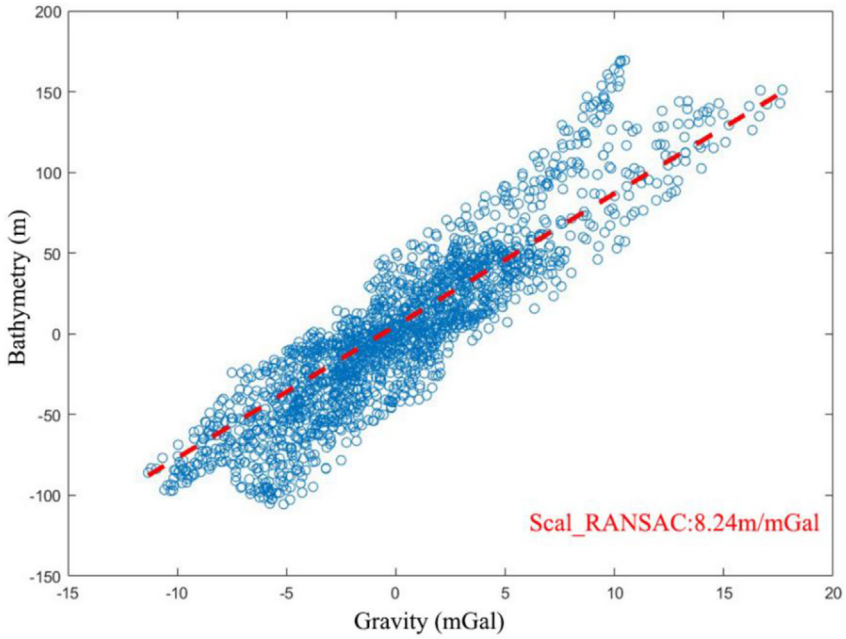

Fig. 5. Illustrations of scaling factor estimations at the sample location.

Table 2
Statistics of the differences between shipborne soundings data in 10 km distances from the coast and the bathymetry derived from Solution A (RANSAC scale factor calculation method) and Solution B (Partition scale factor calculation method) respectively (Units: m).

Method	Max	Min	Mean	STD
Solution A	79.91	−137.78	5.86	31.25
Solution B	79.97	−55.94	16.34	23.91

generated based on the partition scale factor calculation approach can produce higher accuracy results than that acquired using the classic RANSAC scale factor calculation method.

However, we discovered that the resolution of the window established in each divided region is also an influencing factor affecting the final accuracy of the derived coastal bathymetry in the above study when we set the window size of the blocks in the partition scale factor calculation technique. In this way, we pre-selected several window resolutions in the partition method, and different results are computed depending on these distinct resolutions. In this method, the grid resolution is increased from 2′ to 24′ with a 2′ interval for ease of calculation and grid partition. At the same time, shipborne soundings in the along-track 10 km from the coast were used to assess the results. In this way, The STD of the misfits between bathymetry produced on different grid resolutions and soundings data can be used to determine the appropriate grid resolution. The accuracy of the bathymetry derived from different scaling factor grid resolution is shown in Table 3, with a minimum STD of 23.91 m attained when the resolution is chosen as 10′. As 10′ is the appropriate resolution of the grid windows in scaling factor calculation, we use 10′ as the resolution of the grid windows in the following study.

4.3. Coastal bathymetry derived from SAR-based altimetry data

Four types of altimetric gravity models (DTU13GRA, DTU15GRA, DTU17GRA, and DTU21GRA) are employed in modeling the coastal bathymetry in this work to examine the impact of the incorporation of SAR altimetry data on coastal bathymetry modeling. It is worth mentioning that only DTU21GRA included SAR altimetry data compared with DTU13GRA, DTU15GRA, and DTU17GRA. We are primarily interested in determining the accuracy of coastal bathymetry in a 10 km offshore area and comparing the results to shipborne soundings data in this area.

Within 10 km along track distances to the coast, Fig. 6 shows histograms of the disparity between generated from several altimetric gravity models and shipborne soundings data. Clearly, when compared with the results computed from the other three gravity field models, the error distribution of the coastal bathymetry derived from the DTU21GRA gravity model tends to zero, indicating that coastal bathymetry derived from DTU21GRA gravity model is better fit with the coastal seabed topography than that computed from the other three gravity models. Moreover, Table 4 displays the statistical results of the mismatches between coastal bathymetry produced from four altimetry gravity models and data from shipborne soundings. The STD of the misfits derived from DTU21GRA across offshore regions decreases by a magnitude of 1.11 m compared with that calculated from DTU15GRA, and it also decreases by a magnitude of 0.88 m when compared with that calculated from DTU17GRA. These results suggest that the introduction of more CryoSat-2 (low resolution mode) and other altimeter data have an impact on improving coastal bathymetry modeling. However, this impact is much smaller than the improvement in coastal bathymetry modeling from the introduction of SAR altimeter data.

Table 3
The misfits between bathymetry derived from different grid windows resolution and shipborne soundings data.

Resolution (')	2	4	6	8	10	12	14	16	18	20	22	24
Misfits (m)	27.85	25.71	26.13	26.36	23.91	26.37	25.08	26.31	26.60	25.82	25.24	27.54

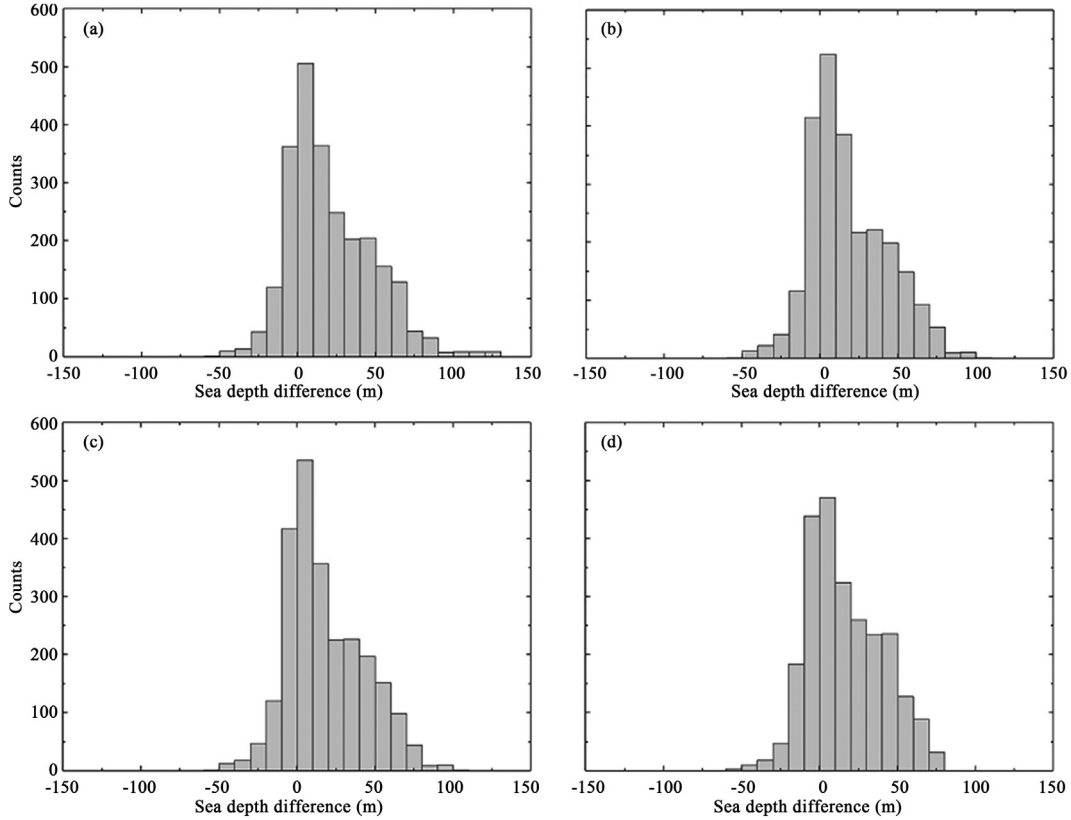

Fig. 6. Histograms of the differences between the coastal bathymetry computed from (a) DTU13GRA; (b) DTU15GRA; (c) DTU17GRA; (d) DTU21GRA and shipborne soundings data.

Table 4
Statistics of the misfits between the modeling coastal bathymetry derived from different gravity field models and shipborne soundings data (in the range from 10 km distances along the track to the coast) (Units: m).

Gravity Field Model	Max	Min	Mean	STD
DTU13GRA	128.29	−51.27	20.73	27.46
DTU15GRA	102.15	−54.97	18.10	25.02
DTU17GRA	100.82	−53.29	17.82	24.79
DTU21GRA	79.97	−55.94	16.34	23.91

In conclusion, the inversion accuracy of the coastal bathymetry model utilizing DTU21GRA is superior to that derived from the other three altimetric gravity models. At the same time, we discovered that the DTU15GRA and DTU17GRA gravity field models' inversion coastline findings were not significantly different. The CryoSat-2 data operated with Geodetic missions and Sentinel-3A/3B data operated with Exact Repeat missions. The GMs make the most contributions to the gravity field due to the high data densities. However, the resolution of ERMs data on each track is much higher than GMs. At the same time, the long-term ERM data can provide accurate average SSHs, though their point densities are low [37]. These results indicate that the long-term ERM data including Sentinel-3A/3B, can improve the accuracy of the gravity model. As a result that the accuracy of the coastal bathymetry model calculated with DTU21GRA can be significantly improved compared with that computed with other gravity models.

We examine the misfits between the bathymetry modeled from these four gravity models and shipborne soundings data in the 5 km along track to the coast, which can help us focus on the influence of the introduction of SAR altimetry data on bathymetry inversion in offshore areas. In the 5 km along the distance to the shore, Fig. 7 demonstrates the misfits between the coastal bathymetry models derived from different altimetry gravity field data and shipborne soundings data. We observe a significant improvement in the coastal bathymetry calculated from DTU21GRA compared with that computed with DTU13GRA, DTU15GRA, and DTU17GRA, especially in Area 1 (from 54.18°S to 54.25°S) and Area 2 (from 54.28°S to 54.37°S). DTU17GRA was computed with more CryoSat-2 data and one year of SARAL data compared with DTU13GRA and DTU15GRA, and this is the main reason that the coastal bathymetry generated from DTU17GRA is superior to that derived from DTU15GRA and DTU13GRA. On the other hand, the DTU21GRA model was developed with Sentinel-3A/3B altimetry SAR data, resulting in a further improvement in coastal bathymetry modeling compared with the other three models.

Moreover, Table 5 shows the statistics of the discrepancies between the coastal bathymetry model obtained from gravity anomaly and shipborne soundings in Areas 1 and 2, from which we can observe that the introduction of Sentinel-3A and Sentinel-3B data may substantially improve the accuracy of the coastal bathymetry in Areas 1 and 2. The STD of the discrepancies between the coastal bathymetry estimated from DTU21GRA and the soundings data in Area 1 is 25.20 m, roughly 0.97 m and 1.51 m lower than that computed from DTU17GRA and DTU13GRA, according to the accompanying statistics results. The coastal bathymetry results for Area 1 calculated from the DTU21GRA show a relative improvement of 3.71% compared with the results computed with the DTU17GRA and a relative improvement of 5.65% compared with the results derived from the DTU13GRA. Concurrently, the STD of misfits calculated from DTU21GRA is 27.52 m in Area 2, which is 2.87 m and 11.53 m lower than that obtained from

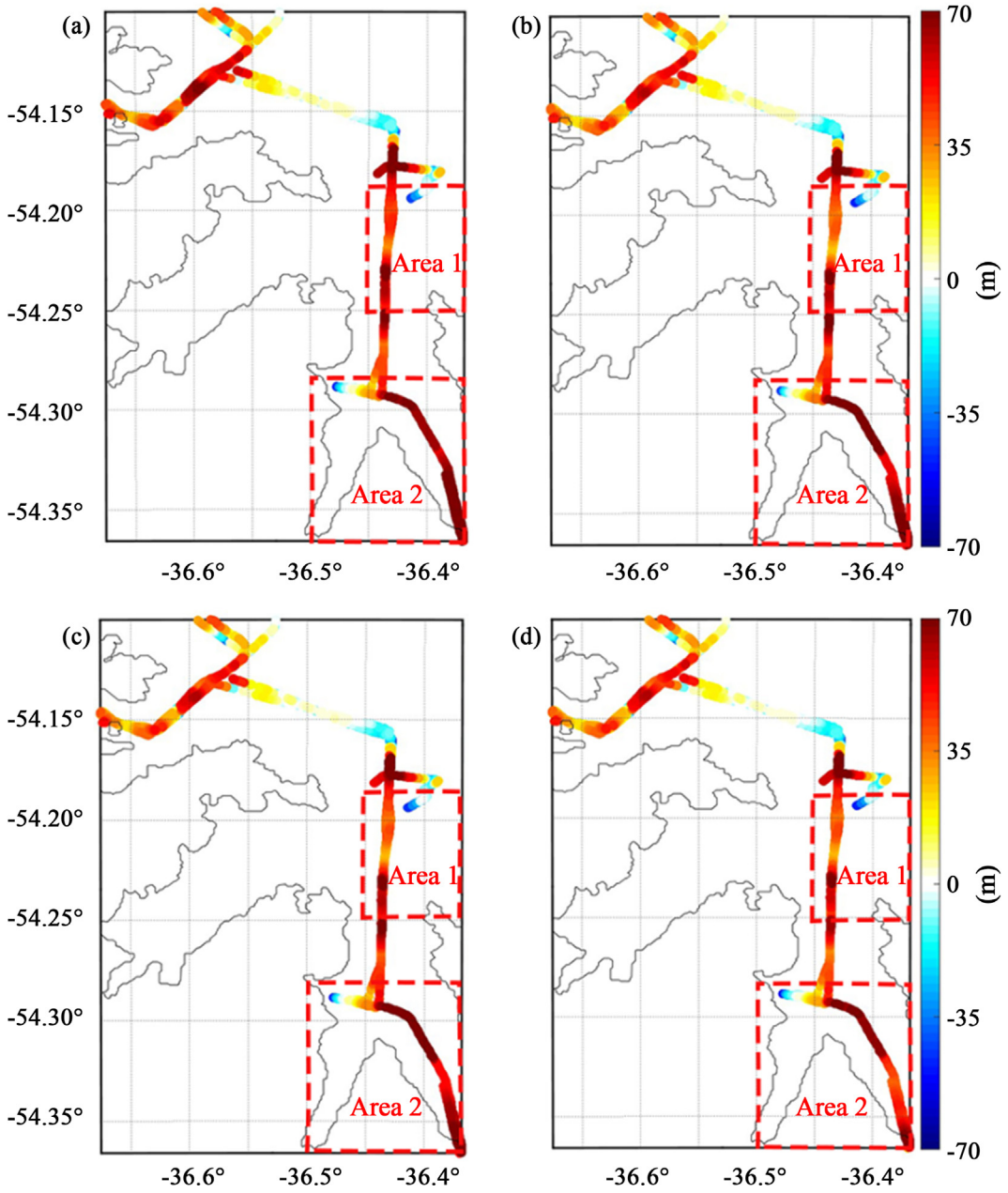

Fig. 7. Misfits between the bathymetry models derived from (a) DTU13GRA; (b) DTU15GRA; (c) DTU17GRA; (d) DTU21GRA and shipborne soundings data (in the range of less than 5 km distances from the coast). The two selected areas in red boxes are the two representative areas.

DTU17GRA and DTU13GRA, respectively. The coastal bathymetry results for Area 2 calculated from the DTU21GRA show a relative improvement of 9.44% compared with the results computed with the DTU17GRA and a relative improvement of 29.53% compared with the results derived from the DTU13GRA.

Table 5
Statistics of the misfits between the modeling coastal bathymetry derived from different gravity field models and shipborne soundings data (in the range of less than 5 km distances along the track to the coast) (Units: m).

Area	Gravity field model	Max	Min	Mean	STD
Area 1	DTU13GRA	78.34	−51.27	36.96	26.71
	DTU15GRA	73.68	−54.97	32.07	26.21
	DTU17GRA	75.86	−53.29	32.82	26.17
	DTU21GRA	68.96	−55.34	30.30	25.20
Area 2	DTU13GRA	128.29	−47.56	55.93	39.05
	DTU15GRA	102.15	−44.59	49.63	30.40
	DTU17GRA	100.82	−46.13	47.91	30.39
	DTU21GRA	79.97	−51.32	38.60	27.52

These results suggest that using SAR altimetry data might considerably improve the accuracy of the coastal bathymetry model. At the same time, we can see that as the distance to the coast increases, the ability of SAR altimetry data to improve the bathymetry model diminishes. Bathymetry modeled from gravity anomaly derived from SAR altimetry data can provide additional details of the seabed topography within 5 km of the coastline.

The coastal bathymetry estimated from SAR-based altimetry data is further evaluated, with data from shipborne soundings serving as the control data. We also evaluate the accuracy of SAR altimetry-derived coastal bathymetry models to other global bathymetry models in the research area (in the range from 10 km distances along the track to the coast). According to the statistics results in Table 6, the STD of discrepancies between coastal

Table 6
Statistics of the differences from shipborne soundings data (in the range from 10 km distances along the track to the coast) analysis (Units: m).

Model	Max	Min	Mean	STD
BAT_DTU21GRA	79.97	−55.94	16.34	23.91
GEBCO2020	77.45	−82.31	11.19	25.73
Topo_DTU18	141.49	−75.79	10.74	30.66
SIO_topo_v20.1	219.60	−193.28	15.65	48.47
SIO_topo_v23.1	221.85	−111.36	14.49	48.39

bathymetry generated from DTU21GRA and shipborne soundings data (in the range of 10 km distances along the route to the coast) is 23.91 m, which is around 1.82 m lower than that estimated from GEBCO2020, and the accuracy of other global bathymetry model in this area is narrower than that of bathymetry modeled from DTU21GRA. This result suggests that utilizing Sentinel-3A and Sentinel-3B data to refine coastal bathymetry is possible.

5. Conclusion

The effects on coastal bathymetry refinement based on SAR altimetry data are quantified and assessed. We refine the local coastal bathymetry model based on the global reference bathymetry model and altimetric gravity data. The bathymetry models computed with different altimetric gravity models are assessed with high-quality shipborne soundings data for external validation.

The bathymetry inversion over the South Sandwich Island reveals that the truncation wavelengths in the band-pass filter impact the bathymetry inversion. The scale factor calculation based on the partition-wise scheme improves the accuracy of the coastal bathymetry, by a magnitude of 7.34 m, compared with that calculated with the RANSAC method. These results show that the method of partition scale factor calculation can receive better precision inversion bathymetry than that obtained by the classic random consistency algorithm. Moreover, the resolution of the partition area block is one of the elements impacting the accuracy of bathymetry inversion in the process of partition scale factor computation.

By introducing the gravity data calculated with the Sentinel-3A and Sentinel-3B, the accuracy of the coastal bathymetry is significantly improved compared with the results computed without SAR altimetry data by a magnitude of 3.55 m. This suggests that using SAR altimetry data such as Sentinel-3A and Sentinel-3B over the coasts of South Georgia and the South Sandwich Islands in the South Atlantic Ocean can significantly improve the accuracy of local bathymetry. Furthermore, the addition of more CryoSat-2 altimetry data can improve the accuracy of the recovered bathymetry model.

It is worth noting that within 5 km of the coast, the bathymetry estimated from gravity anomaly determined from SAR altimetry data is improved, compared with the model calculated from the gravity data computed without SAR altimetry data, by a magnitude of 11.53 m. However, with the increased distances from the offshore area to open sea, the improved bathymetry using SAR altimetry data is weakened.

The introduction of SAR data like Sentinel-3A and Sentinel-3B can reduce the defect of low accuracy of gravity data over coastal areas to effectively improve the accuracy of coastal bathymetry modeling. Bathymetry modeled with SAR altimetry data can provide more details of seabed topography, especially over the shoreline areas. At the same time, the employment of a data fusion method to fuse multi-source data to improve the global bathymetry model is being studied in the future.

Author contributions

Conceptualization, Y.W. and J.W.; methodology, J.W. and Y.W.; software, J.W. and Y.W.; validation, Y.W. and J.W.; formal analysis, Y.W. and J.W.; investigation, Y.W., J.W.; resources, Y.W.; data curation, J.W.; writing—original draft preparation, Y.W. J.W.; writing—review and editing, Y.W., X.H.; visualization, J.W. and D.J.; supervision, X.H. and Y.W.; project administration, Y.W. and Y.S.; funding acquisition, Y.W. All authors have read and agreed to the published version of the manuscript.

Conflicts of interest

The authors declare that there is no conflicts of interest.

Acknowledgments

This study was supported by the National Natural Science Foundation of China (No. 42004008), the Natural Science Foundation of Jiangsu Province, China (No. BK20190498), the Fundamental Research Funds for the Central Universities (No. B220202055), and the State Scholarship Fund from Chinese Scholarship Council (No. 201306270014).

References

[1] P.J. Bart, D. Mullally, N.R. Golledge, et al., The influence of continental shelf bathymetry on Antarctic Ice Sheet response to climate forcing, Global Planet. Change 142 (2016) 87–95, https://doi.org/10.1016/j.gloplacha.2016.04.009.
[2] D.F. Porter, K.J. Tinto, A. Boghosian, J.R. Cochran, R.E. Bell, S.S. Manizade, J.G. Sonntag, Bathymetric control of tidewater glacier mass loss in northwest Greenland, Earth Planet Sci. Lett. 401 (2014) 40–46, https://doi.org/10.1016/j.epsl.2014.05.058.
[3] Christine A. Ribic, Erik Chapman, William R. Fraser, et al., Top predators in relation to bathymetry, ice and krill during austral winter in Marguerite Bay, Antarctica, Deep Sea Res. Part II Top. Stud. Oceanogr. 55 (2008) 485–499, https://doi.org/10.1016/j.dsr2.2007.11.006.
[4] F.O. Nitsche, D. Porter, G. Williams, et al., Bathymetric control of warm ocean water access along the East Antarctic Margin, Geophys. Res. Lett. 44 (2017) 8936–8944, https://doi.org/10.1002/2017GL074433.
[5] H. Burningham, J. French, Seabed dynamics in a lage coastal embayment: 180 years of morphological change in the outer Thames estuary, Hydrobiologia 672 (2011) 105–119, https://doi.org/10.1007/s10750-011-0760-y.
[6] S. Pike, D. Traganos, D. Poursanidis, J. Williams, K. Medcalf, P. Reinartz, N. Chrysoulakis, Leveraging commercial high-resolution multispectral satellite and multibeam sonar data to estimate bathymetry: the case study of the caribbean sea, Rem. Sens. 11 (2019) 1830, https://doi.org/10.3390/rs11151830.
[7] IPBES global assessment preview, Available online: https://www.ipbes.net/news/ipbes-global-assessment-preview. (Accessed 12 June 2019).
[8] B. Tozer, D.T. Sandwell, W.H.F. Smith, C. Olson, J.R. Beale, P. Wessel, Global bathymetry and topography at 15 arc sec: SRTM15+, Earth Space Sci. 6 (2019) 1847–1864, https://doi.org/10.1029/2019EA000658.
[9] C.C. Carabajal, D.J. Harding, J.P. Boy, et al., Evaluation of the global multi-resolution terrain elevation data 2010 (GMTED2010) using ICESat geodetic control, in: International Symposium on Lidar and Radar Mapping 2011: Technologies and Applications, 2011, p. 8286, https://doi.org/10.1117/12.912776.
[10] D.N. Zhao, Z.Y. Wu, J.Q. Zhou, et al., From 10 m to 11000 m, automatic processing multi-beam bathymetric data based on PGO method, IEEE T. Geosci. Remote. 9 (2021) 14516–14527, https://doi.org/10.1109/ACCESS.2021.3051909.
[11] D.T. Sandwell, R.D. Müller, W.H.F. Smith, E. Garcia, R. Francis, New global marine gravity model from CryoSat-2 and Jason-1 reveals buried tectonic structure, Science 346 (2014) 65–67, https://doi.org/10.1126/science.1258213.
[12] S. Zhang, D.T. Sandwell, T. Jin, D. Li, Inversion of marine gravity anomalies over southeastern China seas from multi-satellite altimeter vertical deflections, J. Appl. Geophys. 137 (2017) 128–137, https://doi.org/10.1016/j.jappgeo.2016.12.014.
[13] D.T. Sandwell, W.H.F. Smith, Global marine gravity from retracked Geosat and ERS-1 altimetry: ridge segmentation versus spreading rate, J. Geophys. Res. Solid Earth 114 (2009), https://doi.org/10.1029/2008JB006008.
[14] E.A. Jan, J. Wilfried, D. Boris, et al., A new bathymetry of the Northeast Greenland continental shelf: constraints on glacial and other processes, Geochem. Geophys. Geosyst. (16) (2015) 3733–3753, https://doi.org/10.1002/2015GC005931.
[15] K.H. Tseng, C.K. Shum, Y.C. Yi, et al., The improved retrieval of coastal sea surface heights by retracking modified radar altimetry waveforms, IEEE Trans. Geosci. Rem. Sens. 52 (2014) 991–1001, https://doi.org/10.1109/TGRS.2013.2246572.

[16] R.K. Raney, The delay/Doppler radar altimeter, IEEE Trans. Geosci. Rem. Sens. 36 (1998) 1578–1588, https://doi.org/10.1109/36.718861.
[17] S.B. Yang, H.G. Liu, K. Xu, X.Y. Xu, The mean echo model and data process of SAR altimeter, in: IEEE International Symposium on Geoscience and Remote Sensing (IGARSS), 2011, pp. 2077–2080, https://doi.org/10.1109/igarss.2011.6049573.
[18] N. Galin, D.J. Wingham, R. Cullen, R. Francis, I. Lawrence, Measuring the pitch of CryoSat-2 using the SAR mode of the SIRAL altimeter, IEEE Geosci. Remote Sens. Lett. 11 (2014) 1399–1403, https://doi.org/10.1109/LGRS.2013.2293960.
[19] A. Dossing, T.M. Hansen, A.V. Olesen, et al., Gravity inversion predicts the nature of the Amundsen Basin and its continental borderlands near Greenland, Earth Planet Sci. Lett. 408 (2014) 132–145, https://doi.org/10.1016/j.epsl.2014.10.011.
[20] V.A. Childers, D.C. Mcadoo, J.M. Brozena, et al., New gravity data in the Arctic Ocean: comparison of airborne and ERS gravity, J. Geophys. Res. Solid Earth 106 (2001) 8871–8885, https://doi.org/10.1029/2000JB900405.
[21] K. Xu, P. Liu, L.W. Shi, L. Wang, X.F. Yu, The altimeter precision comparison between SAR mode and conventional mode through airborne experiment, in: IEEE International Symposium on Geoscience and Remote Sensing IGARSS, 2015, pp. 3638–3641.
[22] Y.H. Wu, J.J. Wang, A. Abulaitijiang, et al., Local enhancement of marine gravity field over the spratly islands by combining satellite SAR altimeter-derived gravity data, Rem. Sens. 14 (2022), https://doi.org/10.3390/rs14030474.
[23] S. Labroue, F. Boy, N. Picot, M. Urvoy, M. Ablain, First quality assessment of the Cryosat-2 altimetric system over ocean, Adv. Space Res. 50 (2012) 1030–1045, https://doi.org/10.1016/j.asr.2011.11.018.
[24] P. Bonnefond, O. Laurain, P. Exertier, F. Boy, T. Guinle, N. Picot, S. Labroue, M. Raynal, C. Donlon, P. Femenias, T. Par-rinello, S. Dinardo, Calibrating the sar ssh of sentinel-3a and cryosat-2 over the corsica facilities, Rem. Sens. 10 (2018) 92, https://doi.org/10.3390/rs10010092.
[25] C. Donlon, B. Berruti, A. Buongiorno, M.H. Ferreira, P. Femenias, J. Frerick, P. Goryl, U. Klein, H. Laur, C. Mavrocordatos, et al., The global monitoring for environment and security (GMES) sentinel-3 mission, Remote Sens. Environ. 120 (2012) 37–57, https://doi.org/10.1016/j.rse.2011.07.024.
[26] W.H.F. Smith, D.T. Sandwell, Bathymetric prediction from dense satellite altimetry and sparse shipboard bathymetry, J. Geophys. Res. Earth Surf. 99 (1994) 21803–21824, https://doi.org/10.1029/94JB00988.
[27] M.Z. Hu, J.C. Li, H. Li, et al., Predicting global seafloor topography using multi-source data, Mar. Geodes. 38 (2015) 176–189, https://doi.org/10.1080/01490419.2014.934415.
[28] Q. Li, Li Bao, Comparative analysis of methods for bathymetry prediction from altimeter-derived gravity anomalies, Hydrograp. Surv. Chart. 36 (2016) 1–4.
[29] M.A. Fischler, R.C. Bolles, Random sample consensus: a paradigm for model fitting with applications to image analysis and automated cartography, Commun. ACM 34 (1981) 381–395.
[30] B. Ashalatha, Fractal analysis of gravity and bathymetry profiles across ridges in Indian Ocean, Indian J. Mar. Sci. 36 (2007) 110–116.
[31] S. Zhong, O.Y. Ming, G. Bin, Bathymetry predicting using the altimetry gravity anomalies in South China Sea, Geod. Geodyn. 9 (2018) 156–161.
[32] R.L. Parker, The rapid calculation of potential anomalies, Geophys. J. Roy. Astron. Soc. 31 (1973) 447–455, https://doi.org/10.1111/j.1365-246X.1973.tb06513.x.
[33] A. Abulaitijiang, O.B. Andersen, D. Sandwell, Improved arctic ocean bathymetry derived from DTU17 gravity model, Earth Space Sci. 6 (2019) 1336–1347, https://doi.org/10.1029/2018EA000502.
[34] D.C. Kapoor, General bathymetric chart of the Oceans (GEBCO), Mar. Geodes. 5 (1981) 268–269.
[35] O.B. Andersen, P. Knudsen, The DTU17 global marine gravity field: first validation results, in: International Association of Geodesy Symposia, Springer, Berlin/Heidelberg, Germany, 2019.
[36] Y.H. Wu, A. Abulaitijiang, O.B. Andersen, et al., Refinement of mean dynamic topography over island areas using airborne gravimetry and satellite altimetry data in the northwestern South China sea, J. Geophys. Res. Solid Earth 126 (2021), https://doi.org/10.1029/2021JB021805.
[37] C.C. Zhu, J.Y. Guo, J.Y. Gao, et al., Marine gravity determined from multi-satellite GM/ERM altimeter data over the South China Sea: SCSGA V1.0, J. Geodes. 94 (2020), https://doi.org/10.1007/s00190-020-01378-4.

Yihao Wu received his BSc degree, MSc degree and PhD degree in geodesy from Wuhan University, China, in 2010, 2012, and 2016, respectively. He is an associate professor at the School of Earth Sciences and Engineering, Hohai University, Nanjing, China. His main research areas include physical geodesy and satellite altimetry data processing.

Junjie Wang is an MSc student at the School of Earth Sciences and Engineering, Hohai University, Nanjing, China. His current research mainly focuses on bathymetry modeling.

Xiufeng He received her MSc degree and PhD degree from Nanjing University of Aeronautics and Astronautics and Hong Kong Polytechnic University, respectively. She is a professor at the School of Earth Sciences and Engineering, Hohai University, Nanjing, China. Her main research areas include satellite navigation and positioning, InSAR technology, and deformation monitoring.